# Power Spectra in Global Defect Theories of Cosmic Structure Formation

Ue-Li Pen,[1,*] Uroš Seljak,[2,†] and Neil Turok[3,‡]

[1]*Harvard College Observatory, 60 Garden St., Cambridge Massachusetts 02138*
[2]*Harvard-Smithsonian Center for Astrophysics, 60 Garden St., Cambridge Massachusetts 02138*
[3]*DAMTP, Silver St., Cambridge, CB3 9EW, United Kingdom*
(Received 17 April 1997)

An efficient technique for computing perturbation power spectra in field ordering theories of cosmic structure formation is introduced, enabling computations to be carried out with unprecedented precision. Microwave anisotropy and matter perturbation power spectra for global strings, monopoles, textures, and nontopological textures are presented and compared with recent observations. The most striking results are (a) the absence of pronounced peaks in the $C_l$ anisotropy power spectrum and (b) the lack of large scale power in the matter power spectrum.    [S0031-9007(97)03908-2]

Over the next few years, high resolution maps of the cosmic microwave sky will become available. These maps will allow competing theories of cosmic structure formation to be tested with exquisite precision. The primary quantities of interest for comparing theories to observations are the power spectra of fluctuations, both for the microwave sky temperature and the mass density. The predictions of simple inflationary theories have largely been worked out, typically to 1% accuracy, and detailed comparisons with data are taking place. The state of the main rival set of theories, based on symmetry breaking and phase ordering, has been less rosy. These theories involve a causal source comprising the ordering fields and/or defects, which continually perturbs the Universe on ever larger scales. In the inflationary theories, linear perturbation evolution is all that is needed: but for the defect theories full linear response theory is required. The defect sources are in general "decoherent" [1], providing additional computational difficulty. This Letter presents a general solution method for solving the linear response problem in such models.

*Stiff sources: measuring unequal time correlators.*— Accurate codes have been developed for field evolution in different symmetry-breaking theories. But a single simulation cannot simultaneously resolve all scales of observational relevance. Thus information gathered from simulations must be combined in some way. It has been clear for some that the ideal quantity which (a) uses all the information present in a simulation, (b) incorporates the powerful properties of scaling evolution and causality, and (c) preserves all the information needed to compute power spectra is the unequal time correlator (UETC) of the defect source stress energy tensor $\Theta_{\mu\nu}$:

$$\langle \Theta_{\mu\nu}(\mathbf{k}, \tau)\Theta_{\rho\lambda}(-\mathbf{k}, \tau')\rangle \equiv C_{\mu\nu,\rho\lambda}(k, \tau, \tau'), \quad (1)$$

where $\tau$, $\tau'$ denote conformal time, and $k$ comoving wave number. Because the perturbed Einstein-matter equations are linear, all perturbations are determined in terms of the source via appropriate Green functions. Thus in

principle all quadratic estimators of the perturbations are determined by (1).

The unequal time correlators are highly constrained by causality, scaling, and stress energy conservation. Causality means that the real space correlators of the fluctuating part of $\Theta_{\mu\nu}$ must be zero for $r > \tau + \tau'$ [2]. Scaling [3] dictates that in the pure matter or radiation eras $C_{\mu\nu,\rho\lambda} \propto \phi_0^4/(\tau\tau')^{\frac{1}{2}}c_{\mu\nu,\rho\lambda}(k\tau, k\tau')$, where $\phi_0$ is the symmetry-breaking scale and $c$ is a scaling function. Finally, energy and momentum conservation for the stiff source (see, e.g., [3]) provide two linear constraints on the four scalar components of the source. Any pair determines the other two up to possible integration constants. In our work we have found the best pair to be the energy density $\Theta_{00}$ and the anisotropic stress $\Theta^S$; the energy and momentum conservation equations give good behavior for all components on both superhorizon and subhorizon scales. This choice is also favored by the fact that $\Theta_{00}$ and $\Theta^S$, along with the vector and tensor components, $\Theta^V$ and $\Theta^T$ fix the superhorizon perturbations in the most direct manner. However, we have also checked that other choices give consistent results.

As mentioned, our method uses scaling and causality to extend the dynamic range of the numerical simulations. In the simulations, the fields start from uncorrelated initial conditions, and evolve toward scaling behavior. We evolve the fields to some final time $\tau$ when we compute the stress energy tensor $\Theta_{\mu\nu}$, which we Fast Fourier Transform and decompose into the variables $\Theta_{00}$, $\Theta^S$, $\Theta^V$, and $\Theta^T$. We then repeat the simulation identical initial conditions, computing the same quantities at times $\tau' \leq \tau$. This procedure ensures that correlators are measured when the system is as close to scaling as possible. Correlators are stored as isotropic averages, e.g., $C_{00,S}(k, \tau, \tau') = \langle \Theta_{00}(\mathbf{k}, \tau)\Theta^S(-\mathbf{k}, \tau')\rangle$. Statistical and sampling errors are small at large $k$, but at small $k$ the sampling is sparse and the noise larger. To increase the resolution for small $k\tau$, we compute the correlators in real space as functions of the radial separation $r$. We then make use of the fact that

the correlators vanish for $r > \tau + \tau'$, and transform back to Fourier space $C(k) = 4\pi \int_0^{\tau+\tau'} r^2 dr C(r) \sin(kr)/kr$. For small $k\tau$ we use the latter equation, while for large $k\tau$ we use the direct Fourier space computation. For intermediate values the two match well.

*Eigenvector product representation.*—We have explained how one can devote the full numerical power at hand to compute the UETC's, without wasting computational effort or storage on linear perturbation theory. Next we shall show how fast Einstein-Boltzmann solvers recently developed [4] can be used to convert the UETC's into cosmological power spectra with minimal numerical effort and very high precision.

This is done by representing the UETC's as a sum of eigenvector products [2]. The idea is to regard the stress energy correlators (1) as "symmetric matrices" with indices $\mu\nu, \tau$, and $\rho\lambda, \tau'$. In practice, to compute the scalar perturbations we need the auto- and cross-correlators of two components (for example, $\Theta_{00}$ and $\Theta^S$), and for the vector and tensor perturbations we need the two auto-correlators of $\Theta^V$ and $\Theta^T$. Regarded as matrices, the correlators involved are symmetric and positive definite (expectation values of squares) and so their eigenvalues are all real and positive. Matrix index summation is replaced with an integral $\int d\tau w(\tau)$ with $w(\tau)$ some chosen weighting function. Often the choice of weighting is naturally dictated by scaling and dimensional analysis, but in any case the results were checked to be independent of it. For sensible choices of $w(\tau)$ the trace of the correlators is finite; it follows that there is a convergent series of positive eigenvalues which may be used to index the eigenvector sum. The correlators can then be expressed as an infinite sum

$$C(k, \tau, \tau') = \sum_i \lambda^i v^i(k,\tau) v^i(k,\tau'), \qquad (2)$$

where

$$\int d\tau' C(k,\tau,\tau') v^i(k,\tau') w(\tau') = \lambda^i v^i(k,\tau). \quad (3)$$

The indices labeling the components of the stress tensor are implicit. We have found that the first 15 eigenvectors typically reproduce the unequal time correlators to better than 10%; the effect of including more than 15 on the final power spectra is negligible at the few percent level.

The properties of this representation make it ideal for the purpose of computing cosmological perturbations. Namely, (a) the representation automatically minimizes the "least squares" fit, for a given number of eigenvectors, (b) the eigenvectors individually conserve stress energy, (c) the eigenvectors individually vanish as $\tau$ goes to zero since the correlators $C(k, \tau, \tau')$ vanish for $\tau \ll \tau'$, making specification of the initial conditions trivial, and (d) the contribution of successive eigenvectors to the perturbations converges quickly, as a result both of the decrease in eigenvalue and the increasingly oscillatory nature of the eigenvectors. In particular, the incoherent superhori-

zon ($k\tau < 1$) portion of the correlators is represented by an infinite sum of ever more oscillatory eigenfunctions, which have increasingly little effect on the perturbations. The individual eigenvectors are each fed into a full Boltzmann code [4], and the total perturbation power spectra are then given by the sum of those for individual eigenvectors, weighted by their eigenvalue.

During the pure matter and radiation epochs, the procedure is simplified because the correlators scale, and so are represented for all $k$ by a single set of eigenvectors, functions of $k\tau$. We incorporate the matter-radiation transition by repeating the computation of unequal time correlators for several different values (typically 20) of $\tau/\tau^*$, where $\tau^*$ is the conformal time at matter-radiation equality $\Omega_r(\tau^*) = \Omega_m(\tau^*)$. After the simulations are completed, we collect the results in a matrix of correlators, $\Xi(k\tau, k\tau', k\tau^*)$, which are then diagonalized to produce a set of eigenvectors for each $k\tau^*$ considered. These eigenvectors smoothly interpolate between those for the radiation era and those for the matter era, so the Boltzmann code can use a simple spline interpolation between them. The integration solves the full linearized relativistic Einstein equations tracking the photons, baryons, cold dark matter, and neutrinos. The evolution includes the full matter-radiation transition, finite recombination rate, and other effects. The Boltzmann calculations are accurate to about 1%.

*Checks.*—Many checks have been performed on this procedure, which we briefly summarize here [5]. When the box size of texture simulations is reduced from $400^3$ to $256^3$, the $C_l$ spectrum changes by less than 3%. To check consistency with energy conservation we used a different pair of scalar variables $\Theta_{00} + \Theta$, $\Theta + 2\Theta^S$, which changed the results by 5% in $400^3$ boxes, but gave much slower convergence with box size. Weighting the diagonalization by an additional factor of $\tau^{1/2}$ adds more weight to subhorizon scales, and affects the result by up to 10% at $l = 2$, but less than 2% at larger $l$. We have compared the total, as well as scalar, vector, and tensor anisotropies to those produced by the direct line-of-sight integration code [3], and they individually agree to 10%–20%. Since the current method includes additional contributions at the last scattering surface, explicitly uses scaling, employs far larger box sizes and more accurate integrations, we conclude the results are consistent with the new results being much more accurate. All these checks indicate that the new results for monopoles, textures, and nontopological textures are reliable to better than 10%. We attach greater uncertainty to the results from global strings because of the well-known logarithmic scaling violation due to the string cores, which are not properly resolved in simulations with a comoving lattice.

*Results.*—The scalar microwave anisotropy power spectra for global cosmic string eigenmodes are shown in Fig. 1. Each eigenmode is coherent and shows the expected acoustic peaks [6], but decoherence is manifested
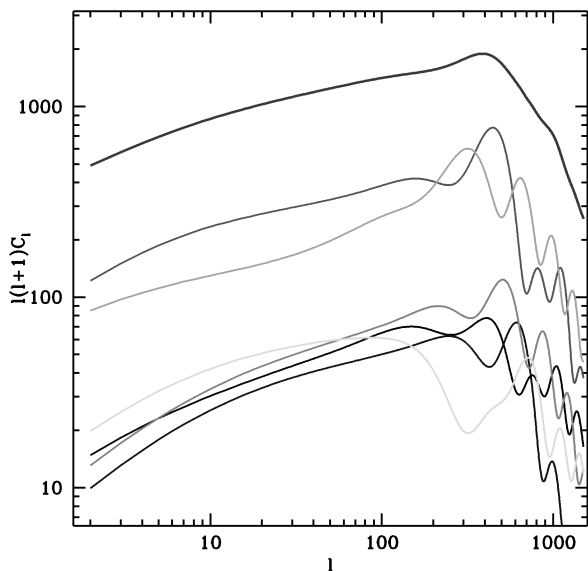
FIG. 1. Angular power spectrum of anisotropies generated by the scalar component of the source stress energy for global strings. The upper curve shows the total spectrum, the lower ones contributions from individual eigenvectors. This figure illustrates decoherence; each eigenvector individually produces an oscillatory $C_l$ spectrum, but these oscillations all cancel in the sum.

in the eigenvector sum. The peaks add out of phase, resulting in a smooth angular power spectrum. One expects cosmic strings to be the least coherent of the defects under consideration. Indeed, the nontopological texture scalar modes do exhibit residual oscillations even when summed over all eigenmodes as shown in Fig. 2. The figures show $C_l$ spectra computed for $h = 0.5$, $\Omega_b = 0.05$, and $\Omega = 1$. The dependence on the Hubble constant $h$ and baryon content $\Omega_b$ is weak [4]. The most striking feature of all the models is the predominance of vector modes. They dominate up to $l \sim 100$, at which point they are suppressed by the horizon size on the surface of last scatter. It is not hard to see that vector and tensor contributions should be at least comparable to the scalar contribution. By causality the $k$ space correlator is an integral over a real space function of compact support, and should be analytic in $k$ at small $k$, and may be Taylor expanded, e.g., $c_{ij,kl}(k\tau, k\tau') = A\delta_{ij}\delta_{kl} + B(\delta_{ik}\delta_{jl} + \delta_{il}\delta_{jk}) + O(k^2)$. The constant $A$ contributes only to trace correlators; $B$ then determines the anisotropic scalar, vector, and tensor contributions, in the ratios $c_{S,S}:c_{V,V}:c_{T,T} = 3:2:4$ (accurately verified in our simulations). Thus vectors and tensors can be expected to contribute a significant fraction of the temperature anisotropies in field ordering theories [4]. The large amplitude of vector modes and the decoherence leads to a suppression of power at $l \gtrsim 100$ [7], a very different result to that from adiabatic fluctuations in inflationary models. We show a comparison between the predictions of the global field defect theories and the current generation of
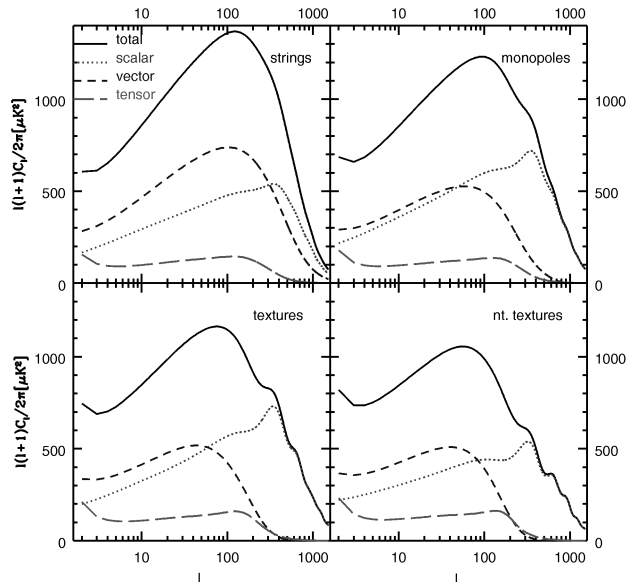


FIG. 2. The contributions to the total power from scalar, vector, and tensor components.

cosmic microwave background (CMB) experiments in Fig. 3. All models are normalized to COBE following Ref. [8]. All are systematically lower than the current degree-scale experimental points.

The same calculations yield the matter power spectra shown in Fig. 4. Normalizing to COBE, we derive $\sigma_8$, the rms mass fluctuation in $8h^{-1}$ Mpc spheres. Global strings, monopoles, texture, and $N = 6$ nontopological texture
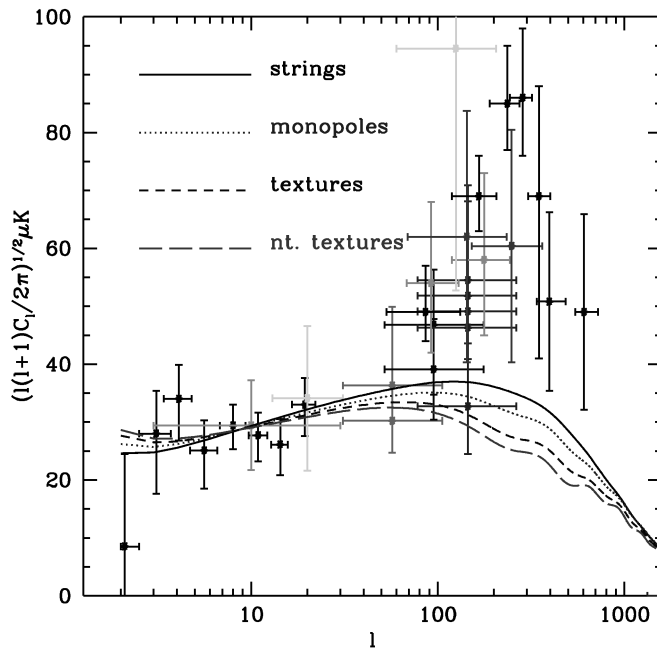


FIG. 3. Comparison of defect model predictions to current experimental data. All models were COBE normalized at $l = 10$.
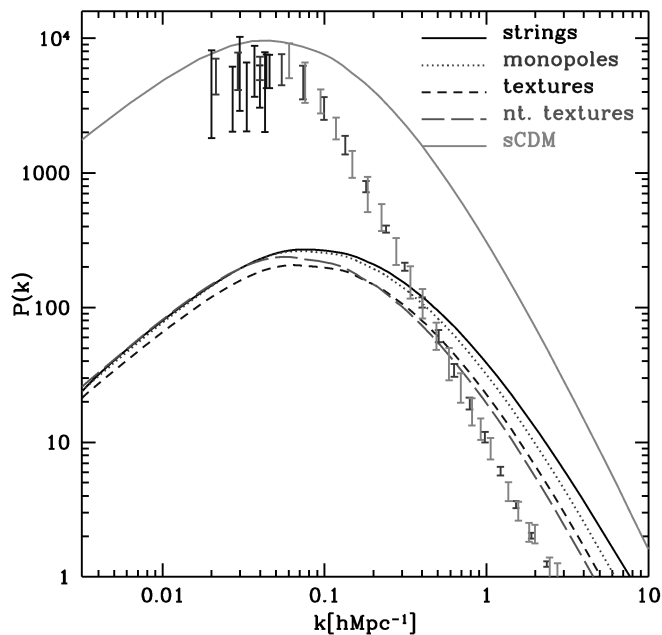
FIG. 4. Matter power spectra computed from the Boltzmann code summed over the eigenmodes. The upper curve shows the standard cold dark matter (sCDM) power spectrum. The defect theories have substantially less power, particularly on large scales, relative to sCDM. All models are normalized to COBE. The data points show the mass power spectrum as inferred from the galaxy distribution [9].

give $\sigma_8 = 0.26$, 0.25, 0.23, and 0.21, respectively, for $h = 0.5$, scaling approximately as $h$. These values for $\sigma_8$ are a factor of 5 lower than the prediction of $n = 1$ inflationary models where $\sigma_8 = 1.2$ for $h = 0.5$. Cluster abundances suggest $\sigma_8 \sim 0.5$ for a flat universe.

Let us briefly comment on the consistency of these results with previous work. The large angle anisotropy results we obtain are consistent at the 10% level with the line of sight integration codes of Pen *et al.* [3] and Coulson *et al.* [10]. The field normalization for textures is $\epsilon = 8\pi^2 G \phi_0^2 = 1.0 \times 10^{-4}$, consistent with our previous calculation [3] of $\epsilon = 1.1 \times 10^{-4}$. We find a slightly larger vector contribution, partly due to our including the matter-radiation transition. The shape of the *scalar* $C_l$ spectrum is broadly consistent with that of [6], but including source decoherence has reduced the amplitude of the Doppler peak relative to the large angle

$C_l$ by a factor of 2, as well as smeared the secondary peaks. The major difference is in the contribution of the vector and tensor $C_l$'s. These were only crudely computed in [6], and strong caveats were given there. The present work must be regarded as superseding the earlier results. The remaining uncertainties are (a) whether we have correctly measured the UETCs and (b) whether the assumption of scaling is valid.

To summarize, the simplest defect models have strongly suppressed acoustic peaks and a low normalization of the matter power spectrum $\sigma_8 \sim 0.25 h_{50}$. Current observations of CMB anisotropies and galaxy clustering do not favor these models. It remains conceivable that the observational data or its interpretation will change. Likewise, some minor modification of the theories might improve matters.

*Electronic address: upen@cfa.harvard.edu
†Electonic address: useljak@cfa.harvard.edu
‡Electronic address: N.G.Turok@amtp.cam.ac.uk

[1] A. Albrecht, D. Coulson, P. Ferreira, and J. Magueijo, Phys. Rev. Lett. **76**, 1413 (1996).
[2] N. Turok, Phys. Rev. D **54**, 3686 (1996); Phys. Rev. Lett. **77**, 4138 (1996).
[3] U. Pen, D. Spergel, and N. Turok, Phys. Rev. D **48**, 692 (1994).
[4] U. Seljak and M. Zaldarriaga, Astrophys. J. **469**, 437 (1996).
[5] U. Pen, U. Seljak, and N. Turok (to be published).
[6] R. G. Crittenden and N. Turok, Phys. Rev. Lett. **75**, 2642 (1995).
[7] Computations for local strings by Allen *et al.* (Report No. astro-ph/9704160) show qualitatively similar results.
[8] E. F. Bunn and M. White, Ap. J. **480**, 6 (1997).
[9] J. A. Peacock, Mon. Not. R. Astron. Soc. **284**, 885 (1997).
[10] D. Coulson, P. Ferreira, P. Graham, and N. Turok, Nature (London) **368**, 27 (1994).